JOURNAL OF CATALYSIS 154, 56–64 (1995)

Effects of Activation on the Surface Properties of Silica-Supported Cobalt Catalysts[1]

Kent E. Coulter and Allen G. Sault

Fuel Science Department 6211, Sandia National Laboratories, Albuquerque, New Mexico 87185-0710

Received October 4, 1994; revised January 20, 1995

Drying and calcining effects on 16–19 wt% Co/SiO_2 Fischer–Tropsch (FT) catalysts, prepared by impregnation with cobalt nitrate, have been examined using ultrahigh vacuum (UHV) surface analysis and conventional catalyst characterization techniques. Drying in air at 110°C or under vacuum at 100°C and then calcining in air at 400°C causes large Co_3O_4 particles to form, which easily reduce under hydrogen at 300°C. In contrast, dried samples annealed under UHV prior to calcining exhibit dramatically different characteristics. The decomposition of cobalt nitrate during drying initiates the formation of a surface cobalt silicate. Prolonged air drying eventually converts the surface silicate into Co_3O_4, while vacuum drying disperses the nitrate precursor on the support, forming cobalt silicate islands. Annealing air-dried samples in UHV stabilizes the surface silicate against reduction or oxidation through the migration of Co^{2+} ions into the support to form a well-ordered bulk cobalt silicate. Annealing of vacuum-dried samples to 200°C in UHV produces a continuous, conductive surface silicate that sinters upon heating to temperatures above 250°C. Analysis of species generated during the decomposition of the $Co(NO_3)_2 \cdot 6H_2O$ precursor indicates that the concentration of gas phase NO_x near the surface determines the nature of the cobalt surface phase. The formation of an intermediate surface cobalt silicate under specific activation conditions maximizes the amount of reducible cobalt surface area available for FT reactions.

1. INTRODUCTION

A wide array of investigations have focused on the behavior of supported cobalt Fischer–Tropsch (FT) catalysts as a function of support (1–6), cobalt dispersion (7, 8), cobalt precursor (9), and pretreatment (10–12). In general, these studies correlate catalytic rates and selectivity with observed cobalt species to assess the effects of preparation and activation on catalyst performance. On alumina, two cobalt species have been identified prior to reduction, and the relative concentrations of these phases determine catalytic performance (13, 14). An easily reducible Co_3O_4 phase is observed for high loadings (>2 wt%) with the relative concentration of this surface species dependent upon the calcination temperature. A second cobalt phase is composed of Co^{2+} ions which have diffused into the support lattice. The relative concentration of these embedded ions increases with increasing calcination temperature and decreasing cobalt loading (6). The Co^{2+} ions occupy tetrahedral and octahedral positions in the Al_2O_3 framework, forming a surface spinel of $CoAl_2O_4$ (15, 16). Temperature-programmed reduction (TPR) profiles of $CoAl_2O_4$ indicate the surface phase does not reduce under H_2 at temperatures below 800°C (17) and the resulting FT activity is minimal (11).

In contrast to the more reactive alumina, silica-supported cobalt catalysts generally possess a Co_3O_4 phase that reduces to metallic Co below 450°C (6). The reduction of Co_3O_4 proceeds through two stages, with Co_3O_4 rapidly reducing to CoO and then to the metal. The rate of CoO reduction depends upon the presence of a support, with supported CoO possessing a higher activation energy for reduction than pure CoO (12). Although SiO_2 is considered an inert support, studies of Co supported on high surface area silicas ($\geq$200 m^2/g) indicate the formation of cobalt silicate surface species that are similar to the aluminates in their resistance to reduction (9, 11, 18, 19). For example, TPR of one of these samples (11) exhibits a high temperature reduction peak at 520°C that is consistent with the formation of a cobalt–silica surface phase during the reduction of Co_3O_4. The CoO intermediate interacts with SiO_2 to form a cobalt silicate surface compound with approximately 35% of the cobalt originally present as Co_3O_4 converting to Co_2SiO_4. The concentration of cobalt migrating into the silica framework depends on the cobalt dispersion and on the number of available tetrahedral defect sites near the surface for incorporation of the Co^{2+} ions. High cobalt dispersions result in a high cobalt silicate concentrations, thereby reducing the amount of easily reducible metal and canceling out the increase in available metallic surface cobalt expected for higher dispersions. These cobalt FT catalysts supported on high surface area silicas exhibit low activities which are rationalized by the small amount of metallic cobalt

[1] This work was performed at Sandia National Laboratories for the U. S. Department of Energy under contract DE-AC04-94AL85000.

0021-9517/95 $6.00

available on the surface of the catalyst following the reduction of Co_3O_4 (11).

Previous reports of support and dispersion effects on cobalt FT activity and selectivity suggest that SiO_2 is an excellent support (1, 2) and that cobalt dispersion does not affect intrinsic catalytic activity (8). A high surface area support loaded with a highly dispersed cobalt phase should therefore optimize FT activity but, as previously discussed, such samples exhibit low activities and a marked reduction dependence on particle size due to the formation of cobalt silicates (11). In order to develop optimum preparation and activation procedures for the formation of Co/SiO_2 catalysts that are both highly dispersed and highly reducible, more detailed studies of metal precursor–support interactions are required. In this paper, the initial results of an investigation of cobalt–support and cobalt–promoter interactions are reported, focusing on the metal–support interactions involved in the decompositon of $[Co(NO_3)_2 \cdot 6H_2O]$ on a silica support under various conditions. A combination of conventional and ultrahigh vacuum (UHV) surface analysis techniques were utilized to investigate the effects of drying and calcining on catalyst properties. The results suggest a novel catalyst activation scheme for Co/SiO_2 catalysts that maximizes the available cobalt metal surface area in the reduced catalyst.

2. EXPERIMENTAL

Two Co/SiO_2 catalysts were prepared by incipient wetness impregnation of SiO_2 (Davisil, grade 643: −200/+425 mesh; 300 m^2/g; 150 Å pores; 1.15 cm^3/g pore volume) with solutions of $Co(NO_3)_2 \cdot 6H_2O$ (Fischer ACS reagent grade) in water (20). Cobalt loadings of 15.8 and 18.8 wt% were obtained after drying and calcining, as determined by atomic absorption spectroscopy.

Incipient wetness impregnation produces bright pink samples that were initially dried in air at room temperature. Once visibly dry, each sample was oven dried to remove residual water. The 15.8 wt% sample was air dried in a static oven at 110°C for 6 h, while the 18.8 wt% sample was vacuum dried at 100°C for 24 h. Following oven drying, the air-dried sample turned black, but the vacuum-dried sample remained pink. A portion of each dried sample was saved for analysis. The remaining allotment of both samples was calcined in a static oven by ramping the catalyst temperature at 5°C/min to 400°C in air and holding at that temperature for 3 h. After calcining, both samples had N_2 BET surface areas of ~230 m^2 per gram of catalyst. The surface area per gram of silica remains unchanged after cobalt loading and calcining, indicating that the cobalt loading procedure did not result in blockage of any pores in the silica. The calcined samples were stored in air following drying and calcining.

Cobalt dispersion was measured by volumetric hydrogen chemisorption at 35°C, using total hydrogen uptake and assuming a 1 : 1 H : Co surface stoichiometry (5). Chemisorption experiments at 100°C give identical results indicating that hydrogen adsorption is not activated for these catalysts. Reuel and Bartholomew (5) also observed that hydrogen uptake is not activated for similar cobalt loadings. Oxygen uptake at 400°C following hydrogen adsorption provides percent reduction (16). Reported dispesions are based on reducible cobalt only, and not the total cobalt loading.

Surface analysis was performed in a UHV chamber (base pressure 3×10^{-10} Torr) coupled to an atmospheric pressure gas-phase reactor. The UHV chamber contains facilities for Auger electron spectroscopy, ion scattering spectroscopy, secondary ion mass spectrometry, x-ray photoelectron spectroscopy (XPS), and temperature programmed desorption. A detailed description of the apparatus is given elsewhere (21). Samples for UHV analysis were prepared by pressing (2000 psi) approximately 30 mg of catalyst onto an etched tungsten mesh (Buckbee–Mears, 0.001-in. wires, 50 wires/in.) to form a porous disk ~0.5 cm in diameter. The sample temperature was monitored by a thermocouple spot-welded to the mesh near the sample.

Pressed samples were introduced to the UHV chamber through the reactor, which is typically evacuated to 5×10^{-7} Torr and outgassed by heating the reactor walls to ~80°C for 4 h prior to opening the valve separating the two compartments. Once in the UHV chamber, samples were analyzed by XPS using AlKα radiation and a VG microtech CLAM2 analyzer at a pass energy of 50 eV, and 4-mm entrance and exit slits. Scans of the Co 2*p*, Si 2*p*, O 1*s*, C 1*s*, and N 1*s* regions were taken, with charging corrections made by referencing to the reported Si 2*p* value of 103.4 eV for SiO_2 (22). In all but one instance, referencing to the Si 2*p* peak results in proper positioning of the C 1*s* peak at 284.6 eV, the typical value for adventitious carbon. For the one case where Si 2*p* referencing results in poor positioning, the C 1*s* peak is used for referencing. The samples were subsequently annealed under vacuum for 5 min at 100, 200, 250, 300, 350, and 400°C to remove any residual surface adsorbates, with an XPS analysis after each anneal. Initially, annealing the samples in a UHV environment was carried out to minimize outgassing of adsorbed impurities in the reactor during activation. In the course of the experiments, however, it was found that UHV annealing strongly influences the surface properties of the dried samples. After UHV annealing, the order of subsequent reduction and calcination steps was determined by the catalyst treatment prior to introduction into UHV. Samples calcined prior to insertion into UHV were first reduced in 630 Torr of hydrogen for 2 h at increasing temperatures (250–400°C) and then

calcined in 130 Torr of O_2 for 1 h at various temperatures (300–400°C). XPS analysis was performed after each treatment. Dried, uncalcined samples were first calcined under 130 Torr oxygen following the vacuum anneal and subsequently reduced under 630 Torr hydrogen at 250–400°C. In addition, repeated cycling between reduction and oxidation steps was carried out on selected samples. Each sequence of treatments was performed on multiple samples in order to ensure the consistency and reproducibility of the results.

For clarity, samples are referred to in the text by the sequence of treatments received. For example, an air-dried, vacuum-annealed, calcined sample refers to a sample which was sequentially air dried, then vacuum annealed, and finally calcined. A vacuum-dried, calcined sample refers to a sample which was vacuum dried and then calcined without an intervening vacuum anneal. Unless otherwise noted, vacuum annealing always refers to heating to 400°C in UHV, while calcining was performed at 400°C in either atmospheric air or 130 Torr oxygen. Air calcining was used for all samples calcined prior to introduction into UHV, while oxygen calcining was used for all calcining treatments performed *in situ* in the atmospheric reactor coupled to the UHV chamber. The two calcining methods give identical results, provided the prior treatment of the samples is also identical.

Reference Co 2*p* spectra for metallic cobalt, CoO, and Co_3O_4 are shown in Fig. 1 to provide peak shapes and binding energies. The $2p_{3/2}$ peak positions are 778.6 eV for metallic cobalt, 780.6 eV for CoO, and 780.0 eV for Co_3O_4. These spectra were acquired from a Co foil (Goodfellow, 99.9% purity) cleaned and prepared using established procedures, and agree well with literature spectra (22–25). The differences among the spectra in Fig. 1 are discussed in detail in reference (23) and further comments on these features as they relate to the supported catalysts are made later in this paper. As a result of the considerable assumptions (background subtraction, mean free paths, line shapes, etc.) required for quantitative analysis of supported catalysts by XPS (12), calculations of elemental atomic ratios are not incorporated into this study, although qualitative comparisons of Co $2p_{3/2}$/Si 2*p* intensity ratios are made and shown in Table 1. All Co 2*p* XPS spectra shown are adjusted to give equal $2p_{3/2}$ peak heights.

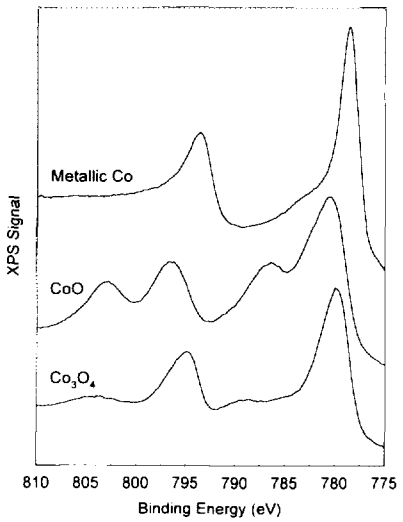

FIG. 1. Co 2*p* XPS spectra for metallic cobalt, CoO, and Co_3O_4.

3. RESULTS AND DISCUSSION

A. Air-Dried, Calcined Catalyst

The Co 2*p* region of the 15.8 wt% Co/SiO_2 catalyst after air drying and calcining is shown in Fig. 2. The as-prepared spectrum exhibits cobalt features indicative of a Co_3O_4 surface phase with a Co $2p_{3/2}$ peak at 779.8 eV and very small shakeup features. Annealing the sample under vacuum to 400°C increases the Co $2p_{3/2}$/Si 2*p* inten-

TABLE 1

Co/Si Ratios[a]

Treatment	A. Air dried, calcined	B. Air dried	C. Vacuum dried, calcined	D. Vacuum dried
As-prepared	1.08	0.85	0.55	4.95
200° vacuum	1.13	0.92	0.64	5.84
300° vacuum	1.23	1.00	0.58	7.13
400° vacuum	1.34	1.12	0.70	6.55
Reduced at 250°C	1.48	NA	0.67	NA
Oxidized at 400°C	1.49[b]	1.03	NA	4.61
Reduced at 250°C	1.72	0.92	NA	NA
Reduced at 400°C	NA[c]	0.72	NA	3.68

[a] Ratios are based on Co $2p_{3/2}$ and Si 2*p* peak areas using a linear background subtraction. Ratios are not elemental atomic ratios and are only relevant for comparison between samples in this paper.

[b] The air-dried, calcined sample was oxidized at 300°C.

[c] Not applicable.

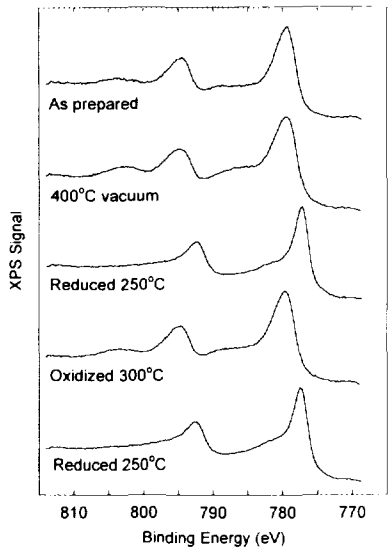

FIG. 2. Co 2*p* XPS spectra for an air-dried, calcined sample as prepared, then sequentially vacuum-annealed at 400°C for 5 min, reduced at 250°C for 2 h, calcined at 300°C for 1 h, and reduced at 250°C for 2 h. All Co 2*p* XPS spectra are adjusted to give equal $2p_{3/2}$ peak heights.

sity ratio and enhances the shake-up feature at 787 eV that is associated with CoO (23). These findings are consistent with literature reports (24) of Co_3O_4 reduction under high temperature UHV conditions. Residual gas analysis (RGA) during the anneal identifies water as the major desorbing species with trace amounts of NO_x also observed. Reduction at 250°C shifts the cobalt peak to the metallic binding energy of 778.4 eV and no other Co surface phases are detectable. The complete reduction of cobalt for an air-dried, calcined sample agrees well with the XPS results of Castner and Santilli (6) for a silica-supported cobalt catalyst prepared under similar conditions. Although XPS indicates complete cobalt reduction, oxygen uptake at 400°C suggests that ~10% of the cobalt is not reduced at 300°C. The discrepancy between XPS and oxygen uptake results from the surface sensitive nature of XPS. Hydrogen chemisorption measures a cobalt dispersion of ~6% for this sample, indicating the average cobalt particle is large (~20 nm). Atoms located in the center of the particles are therefore not probed by XPS due to the relatively short escape depth (1.4 nm (22)) of the cobalt 2*p* photoelectrons. As a result, a small core of unreduced cobalt in the particles would not be seen by XPS. Increasing the reduction tempeature to 400°C does not affect the $2p_{3/2}$ peak shape or position, although a small decrease in the Co signal suggests sintering of the metal. Calcining the reduced sample increases the Co intensity slightly and returns the cobalt to Co_3O_4 that reduces easily (250°C) and has properties identical to the Co_3O_4 in the as-prepared sample. Cycling the catalyst through reduction and oxidation steps increases the Co $2p_{3/2}$/Si 2*p* ratio either through redispersion or emergence of cobalt from silicate sites within the silica framework, although this increase in cobalt intensity is small.

B. Air-Dried Catalyst

The air-dried sample exhibits dramatically different cobalt XPS features from the air-dried and calcined sample. As shown in Fig. 3 for an uncalcined air-dried sample, the as-prepared spectrum shows a higher Co $2p_{3/2}$ binding energy (780.8 eV) than the calcined sample, larger peak widths, and greater intensity in the shakeup features. The large peak widths suggest the presence of at least two distinct cobalt phases, with binding energies higher and lower, respectively, than the Co $2p_{3/2}$ peak position of 780.8 eV. Comparison with the cobalt oxide spectra in Fig. 1 indicates that one of the phases could be Co_3O_4, but that the $2p_{3/2}$ binding energy of CoO is not high enough to account for the second phase. The second component is identified as a cobalt silicate, since these compounds are known to have Co $2p_{3/2}$ binding energies of ~781.5 eV (22). The symmetrical nature of the Co $2p_{3/2}$ peak of the as-prepared sample suggests that the two components are present in roughly equal amounts.

Similar studies on zirconia promoted silica-supported cobalt catalysts are in progress, and preliminary results from these catalysts support a sequential transition from a nitrate precursor to a surface silicate to Co_3O_4 during air drying at 100°C. The relative concentration of the two cobalt phases depends upon the length of drying for the ZrO_2 promoted catalysts. For example, a sample air dried for 3 h exhibits cobalt features of a mixture of surface silicate and Co_3O_4 similar to those in Fig. 3 for a Co/SiO_2

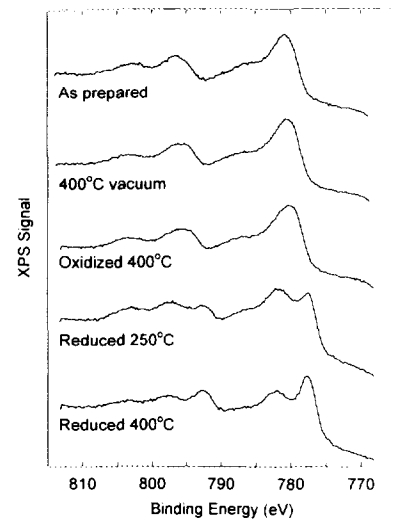

FIG. 3. Co 2*p* XPS spectra for an air-dried sample as prepared, than sequentially vacuum-annealed at 400°C for 5 min, calcined at 400°C for 1 h, reduced at 250°C for 2 h, and reduced at 400°C for 2 h. All Co 2*p* XPS spectra are adjusted to give equal $2p_{3/2}$ peak heights.

sample air dried for 6 h, but if the sample is air dried for 21 h at 110°C, the Co 2*p* features are more indicative of Co_3O_4. This dependence upon drying time suggests the decomposition of $Co(NO_3)_2 \cdot 6H_2O$ in air is kinetically limited and the thermodynamically favored cobalt phase under these conditions is Co_3O_4. These results are in agreement with thermal decomposition studies of unsupported cobalt nitrate hexahydrate in air (26).

Annealing the unpromoted air dried sample under vacuum to 400°C shifts the binding energy of the Co $2p_{3/2}$ peak to 780.4 eV and lowers the shake-up intensity. Water is the main gas phase species generated during annealing, along with trace amounts of NO_x. Following the vacuum anneal, calcining in the UHV reactor cell does not affect the Co 2*p* region as shown in Fig. 3, indicating that both surface silicate and Co_3O_4 are still present. Vacuum annealing prior to calcining is the only difference between the as-prepared sample in Fig. 2 and the calcined sample in Fig. 3. Vacuum annealing therefore stablizes the surface cobalt silicate against further oxidation to Co_3O_4. The resistance of the cobalt to oxidation is proposed to result from the conversion of a disordered surface silicate to a well-ordered bulk silicate during vacuum annealing.

Vacuum annealing prior to calcining also affects the reduction properties of the air-dried catalyst, as shown by comparison of Figs. 2 and 3. For an air-dried, vacuum-annealed, and calcined sample, reduction at 250°C results in two Co $2p_{3/2}$ peaks at 780.8 and 777.6 eV, corresponding to Co^{2+} and metallic cobalt. Higher reduction temperatures increase the relative intensity of the metal peak, although ionic features remain even after 6 h at 400°C under H_2. Reduction of an air-dried, vacuum-annealed sample prior to calcining (not shown) results in a Co 2*p* spectrum similar to the air-dried, vacuum-annealed, and calcined sample, indicating a mixture of silicate and oxide. This result is expected since calcining the air-dried, vacuum-annealed sample does not change the chemical state of the cobalt, as determined by XPS. Reduction of the air-dried sample prior to either vacuum annealing or calcining is easier than reduction of the air-dried, vacuum-annealed sample, with complete conversion to metallic cobalt occurring after 2 h at 300°C under H_2. The higher resistance to reduction of the air-dried, vacuum-annealed sample relative to the air-dried, or air-dried, calcined samples supports the argument for a strongly bound cobalt intermediate, such as a surface silicate, that is stabilized by vacuum annealing. The variable reduction properties of the cobalt surface phases agree well with TPR results (11, 19).

C. *Vacuum-Dried, Calcined Catalyst*

To illustrate the effects of different drying environments on the cobalt surface properties, the vacuum-dried sample was subjected to the same annealing, calcining, and reducing treatments as the air-dried sample. After calcining in air, the vacuum-dried sample exhibits behavior similar to that shown in Fig. 2 for the air-dried and calcined catalyst. Initially, the Co is present as Co_3O_4 that easily reduces and subsequent oxidation–reduction cycles increase the cobalt signal, again suggesting an increase in the amount of metal present on the surface. Rosynek and Polansky (9) observed similar results for a silica-supported cobalt sample that had been vacuum-dried at 60°C for 16 h and calcined in oxygen at 500°C for 16 h. Chemisorption measurements find no significant difference in dispersion (~6%) between the air-dried and calcined, and vacuum-dried and calcined samples, although oxygen uptake following reduction at 300°C indicates approximately 20% of the cobalt on the vacuum-dried, calcined sample is not reduced, versus 10% on the air-dried, calcined sample. In addition, following calcining the intensity of the cobalt XPS signal on the vacuum-dried sample is only half that of the air-dried sample. While the difference in percent reduction is not significant, the difference in Co 2*p* intensity requires explanation. During cobalt impregnation, slightly different procedures were used for the two samples. For the air-dried sample, an amount of water equal to the pore volume was used, while a 50% excess of water was used for the vacuum-dried sample. The higher water content for the vacuum-dried sample may have resulted in a more uniform spatial distribution of cobalt throughout the 30–70-μm particles and a lower cobalt concentration in the near surface region probed by XPS. Grinding of the two samples to reduce the particle sizes to 5–10 μm produces a fivefold decrease in the cobalt signal, confirming that the cobalt is located predominately in the outer layers of the silica particles. Since in neither sample is the cobalt uniformly distributed, it is highly probable that the higher water content used during preparation of the vacuum-dried sample resulted in somewhat greater penetration of cobalt into the pores and a lower concentration of cobalt near the particle surfaces.

D. *Vacuum-Dried Catalyst*

Just as the air-dried sample is very different from the air-dried and calcined sample, the vacuum-dried sample is also very different from the vacuum-dried, calcined sample. As shown in Fig. 4, the vacuum-dried sample exhibits a single Co $2p_{3/2}$ peak at a binding energy of 781.6 eV with a large shake-up feature. Although the binding energy is too high to be due to a cobalt oxide, the large shake-up feature indicates a Co^{2+} species. Comparison with a spectrum of $Co(NO_3)_2 \cdot 6H_2O$ (not shown) gives good agreement and the Co 2*p* spectrum of the vacuum-dried sample is therefore assigned to partially decomposed cobalt nitrate. Further evidence for this assignment

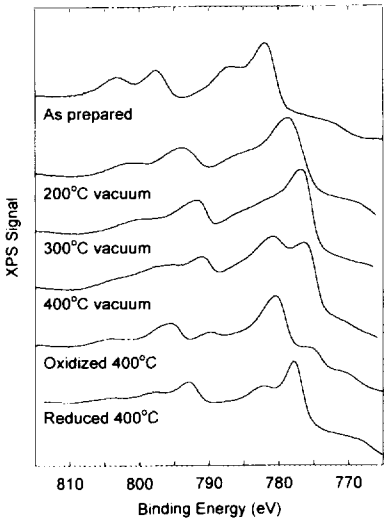

FIG. 4. Co 2*p* XPS spectra for a vacuum-dried sample as prepared, then sequentially vacuum-annealed at 200, 300, and 400°C for 5 min, calcined at 400°C for 1 h, and reduced at 400°C for 2 h. All Co 2*p* XPS spectra are adjusted to give equal $2p_{3/2}$ peak heights.

is provided by the N 1*s* region which shows large amounts of nitrate (406.8 eV) remaining on the surface in contrast to all other samples studied which show no evidence of nitrate. The relative N 1*s*/Co $2p_{3/2}$ intensity ratio is considerably lower than the observed intensity ratio for $Co(NO_3)_2 \cdot 6H_2O$ and supports the assumption that considerable, but not complete, nitrate decomposition has occurred. The cobalt signal on the vacuum-dried sample is 5 times greater than the air-dried sample and 10 times greater than the vacuum-dried, calcined sample. The high cobalt surface coverage prior to calcining indicates vacuum drying either limits the amount of cobalt migrating into the support or dramatically increases dispersion. As mentioned earlier, a visible difference between the air-dried and vacuum-dried samples is the color of the samples. The vacuum-dried samples remain pink after the drying step while the air-dried catalyst turns black. The color difference in conjunction with the observed nitrate peaks in the N 1*s* region suggests that vacuum drying drives off the water and initiates nitrate decomposition but a significant amount of cobalt nitrate remains octahedrally coordinated, giving rise to the pink color (27).

Annealing the vacuum-dried sample in UHV first turns the sample purple and then black with increasing temperature and results in unexpected changes in the Co 2*p* features, as shown in Fig. 4. Vacuum annealing at 200°C for 5 min broadens and shifts the Co $2p_{3/2}$ peak to 779.2 eV and vacuum annealing at 300°C further shifts the peak to 777.8 eV. At 400°C, the Co $2p_{3/2}$ peak splits into two poorly resolved components at 781.8 and 777.2 eV. The Si 2*p* region (Fig. 5) also exhibits unexpected changes during vacuum annealing. Before vacuum annealing, the Si 2*p* spectrum of the vacuum-dried sample indicates the presence of only SiO_2 with a binding energy of 103.4 eV which is used as the reference peak for charge correction. In parallel with the observed shifts in the Co $2p_{3/2}$ binding energy as the vacuum anneal temperature is increased to 200°C, the Si 2*p* peak shifts to 99.6 eV. In this case binding energies are referenced to the C 1*s* peak at 284.6 eV rather than Si 2*p* peak at 103.4, since broadening of the Si 2*p* suggests the presence of more than one silicon species. As a result, use of the Si 2*p* peak position as a reference is doubtful. After vacuum annealing to 300 or 400°C, two well-resolved peaks are apparent in the Si 2*p* region. The higher binding energy peak is assigned to SiO_2 and given a binding energy of 103.4 eV, a reasonable assignment since SiO_2 is expected to possess a higher binding energy than any other silicon species that could be present (22). This assignment places the lower binding energy peak at ~99 eV, a value typical of elemental silicon (22). Coupled with the low binding energy Co $2p_{3/2}$ peak near the value expected for metallic cobalt, it is tempting to postulate the presence of a cobalt silicide. Examination of the O 1*s* region (not shown) discounts this possibility, however. Like the Co 2*p* and Si 2*p* regions, the O 1*s* region also shows an unusually low binding energy peak at ~528 eV, in addition to peaks at 532.6 and 530.0 eV that correspond to SiO_2 and cobalt oxides, respectively (22). Since the low binding energy O 1*s* peak is inconsistent with cobalt silicide formation, and the difference in binding energies between high and low energy peaks is identical for the O 1*s*, Co 2*p*, and Si 2*p* regions, a differential charging effect must be operative. In the absence of any charge correc-

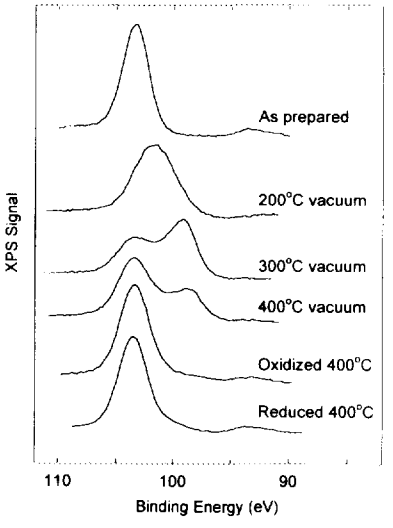

FIG. 5. Si 2*p* XPS spectra for a vacuum-dried sample as prepared, then sequentially vacuum-annealed at 200, 300, and 400°C for 5 min, calcined at 400°C for 1 h, and reduced at 400°C for 2 h. All Si 2*p* XPS spectra are adjusted to give equal 2*p* peak heights.

tions, the low binding energy Co $2p_{3/2}$, Si $2p$, and O $1s$ peaks lie at binding energies expected for cobalt silicate. Thus, both poorly grounded and well grounded silicate layers must exist in the vacuum-dried, vacuum-annealed sample.

The absence of bulk charging and the high Co $2p_{3/2}$/Si $2p$ intensity ratios measured for the vacuum-dried, vacuum-annealed sample suggest a thin layer of silicate is well dispersed over the silica support. A portion of the silicate could be well grounded through direct contact with the tungsten mesh supporting the sample, provided the layer is both continuous and conductive. The conductive nature of the surface cobalt silicate is provided by crystal field theory. For cobalt silicate with seven $3d$ electrons, the splitting of the t_{2g} and e_g bands results in a high-spin complex with a partially filled t_{2g} band, and the resulting material possesses noninsulating properties (28). The changes in the relative intensities of the two silicate peaks with temperature is rationalized by the formation and growth of the highly dispersed silicate layer at low annealing temperatures, followed by sintering of the silicate layer at high temperatures, resulting in discontinuity in the silicate layer and a consequent decrease in the fraction of the silicate which is well grounded. Thus, the sizes of the low binding energy peaks in Figs. 4 and 5 proceed through a maximum with temperature.

RGA during the 200 and 300°C vacuum anneals shows the major desorbing species to be NO, O_2, N_2O, and NO_2 in order of decreasing intensity, with relatively little H_2O, which is the major desorbing species for all other samples. The evolution of NO, O_2, N_2O, and NO_2 in parallel with silicate formation suggests that the surface silicate is formed during the decomposition of cobalt nitrate. In studies (17, 29) on the effects of preparation conditions on the reduction behavior of Co/Al_2O_3 catalysts, the concentration of gas phase NO_2 present that can oxidize Co^{2+} to Co^{3+}, determines the probability of cobalt-aluminate formation. X-ray diffraction indicates that after drying in air at 65°C, the cobalt is well dispersed as small droplets of $Co(NO_3)_2$. Upon calcining at 300°C in the absence of NO_2 these nitrate droplets decompose to form Co^{2+} ions that disperse over the surface and diffuse into the support lattice to form a surface aluminate. In contrast, in the presence of NO_2, Co^{2+} oxidizes to Co^{3+}, preventing this dispersion and forming large Co_3O_4 crystallites. The same argument may explain the trends observed in this study of silica-supported cobalt catalysts. For catalysts that are air dried and calcined in a static oven, NO_2 generated by $Co(NO_3)_2$ decomposition oxidizes the surface silicate to Co_3O_4. *In situ* FTIR analysis of the catalyst during calcining in static air indicates a large surface concentration of NO_x, supporting this contention. The vacuum-dried catalysts that are calcined in a static air oven also follow this pattern of oxidation to Co_3O_4. The large decrease in cobalt XPS intensity that occurs during calcining of the dried catalysts result from the formation of large Co_3O_4 particles, predicted from the presence of NO_x. The vacuum-dried sample contains substantially more nitrate than the air-dried sample, as evidenced by the relative nitrate N $1s$ intensities and the observed rates of NO_x generation during vacuum annealing, and therefore undergoes more extensive cobalt oxidation and Co_3O_4 particle formation. This effect could contribute to the lower Co $2p_{3/2}$ intensity observed for the vacuum-dried, calcined sample relative to the air-dried, calcined sample, although the differences in the spatial distribution of cobalt, which were discussed earlier, are believed to be the primary cause of the lower intensity. Annealing under UHV conditions prior to calcining removes NO_x during $Co(NO_3)_2$ decomposition and the conversion of silicate to Co_3O_4 does not occur. FTIR analysis of a vacuum-dried sample during annealing under vacuum conditions indicates no detectable NO_x species on the surface or in the gas phase.

After calcining the vacuum-dried, vacuum-annealed sample at 400°C, the Si $2p$ region shows only a single peak assigned to SiO_2 at 103.4 eV and no evidence for differential charging. The major Co $2p_{3/2}$ peak is at a charge-corrected binding energy of 780.4 eV (Fig. 4), which is 1.2 eV lower than the reported bulk silicate peak (22). A small Co $2p_{3/2}$ peak remains at the grounded silicate position. Calcining evidently further sinters the highly dispersed silicate phase and greatly decreases the fraction of the silicate that is grounded. The 780.4 eV cobalt binding energy is similar to the binding energy observed for the air-dried, vacuum-annealed sample that is assigned to a mixture of Co_3O_4 and silicate species. The relative XPS intensity of the cobalt features following vacuum annealing and calcining remains approximately an order of magnitude higher than the cobalt signal from the vacuum-dried and oven-calcined sample. Vacuum annealing appears to stablize the highly dispersed cobalt phase of the vacuum-dried, vacuum-annealed sample against sintering during calcining.

Reduction of the oxidized sample in hydrogen is relatively easy, with a metallic Co $2p_{3/2}$ peak observed at reduction temperatures as low as 250°C and a strong metal peak following 400°C reduction (Fig. 4). A high binding energy shoulder remains at ~781 eV, indicating the presence of an irreducible cobalt silcate phase. A similar result is obtained upon reduction of the vacuum-dried, vacuum-annealed sample that has not been calcined.

The vacuum-dried, vacuum-annealed, and reduced sample exhibits the highest Co $2p_{3/2}$/Si $2p$ ratio of any reduced sample studied, suggesting the formation of a highly dispersed surface silicate that maximizes available metallic cobalt surface area. Chemisorption experiments confirm this conclusion. Table 2 shows that hydrogen uptake on a vacuum-dried, vacuum-annealed, reduced

TABLE 2

Hydrogen Chemisorption on Co/SiO_2 Catalysts

Sample[a]	15.8% Co/SiO_2	18.8% Co/SiO_2	18.8% Co/SiO_2
Drying procedure	Air, 100°C, 6 h	Vacuum, 110°C, 23 h	Vacuum, 110°C, 23 h
Vacuum annealing	None	None	400°C, 5 min
Calcining	400°C, 3 h	400°C, 3 h	None
Reduction	H_2, 300°C, 2 h	H_2 300°C, 2 h	H_2, 400°C, 2 h
Total H_2 uptake (cc STP/g · catalyst)	1.54	1.61	2.87
% Reduction[b]	89	79	79
Cobalt dispersion[c]	5.8	5.7	10.1

[a] Percent cobalt determined on dried and calcined samples.
[b] Measured by oxygen uptake at 400°C following hydrogen uptake measurements.
[c] Based on reducible cobalt.

sample is nearly twice that observed on the vacuum-dried, calcined or air-dried, calcined samples. Cobalt dispersion based on reducible cobalt is 10.1%, again nearly twice the values observed for the samples calcined without vacuum annealing. Thus, vacuum drying followed by vacuum annealing results in much smaller cobalt particles and much greater total cobalt surface area than any other activation treatment studied. These findings suggest that to optimize the cobalt surface area of Co/SiO_2 catalysts the formation of a highly dispersed cobalt silicate phase is desirable. The activation conditions that best achieve this goal consist of vacuum drying at 100°C followed by vacuum annealing at 400°C and subsequent reduction under hydrogen at 400°C. The traditional activation treatment of drying in air or under vacuum, followed by calcination and reduction, produces inferior results. Presently, activation treatments and parallel slurry-phase FT reaction studies (30) are in progress, which will extend the activation studies reported here for small (25 mg) catalyst samples to large (~50 g) catalyst samples and allow the beneficial effects of vacuum annealing on FT activity to be quantified. Since annealing large samples in UHV is impractical, annealing to 400°C in flowing helium at high space velocities will be used to simulate the UHV environment and produce large hatches of Co/SiO_2 catalysts with improved cobalt dispersion.

4. CONCLUSIONS

The surface properties of silica supported cobalt catalysts for FT synthesis, prepared by incipient wetness impregnation with a cobalt nitrate precursor, exhibit a strong dependence upon the environment associated with various drying and calcining pretreatment procedures. Calcining in air at 400°C after drying in air or under vacuum at ~100°C forms a Co_3O_4 surface phase that easily reduces. Annealing air- or vacuum-dried samples in UHV prior to calcining stablizes an intermediate cobalt silicate surface phase that is formed during the initial decomposition of the cobalt nitrate precursor. During vacuum annealing, air-dried samples form an irreducible cobalt phase attributed to the migration of Co^{2+} ions into the silica framework. Vacuum-dried samples have a large concentration of nitrate remaining on the surface and heating to 200°C under UHV conditions promotes the decomposition of the precursor to form a continuous, highly dispersed, conductive surface silicate. More specific details regarding the ambient conditions necessary to achieve this continuous silicate film will be presented in a forthcoming publication (31). The nature of cobalt on a silica support is determined by the concentration of surface and gas phase NO_x species during the decomposition of the cobalt nitrate precursor. Large concentrations of NO_x oxidize the intermediate Co^{2+} ions to form large Co_3O_4 particles, whereas in the absence of NO_x the cobalt ions react with the silica to form a surface silicate. The highest dispersions of reducible cobalt supported on silica, are generated by drying at 100°C under vacuum, followed by vacuum annealing at 400°C to form a highly dispersed cobalt silicate, and subsequent reduction at 400°C. This activation procedure results in twice the concentration of cobalt surface area than the more conventional procedure of air drying, followed by calcination and reduction.

ACKNOWLEDGMENTS

The authors thank Elaine Boespflug and Mark Harrington for preparing the catalyst samples studied in this work, and Nancy Jackson, Steve Kohler, and Calvin Bartholomew for stimulating technical discussions. This work was supported by the National Renewable Energy Laboratories under contract RAC 3-13250.

REFERENCES

1. Vannice, M. A., *J. Catal.* **37**, 449 (1975).
2. Vannice, M. A., *J. Catal.* **50**, 228 (1977).

3. Bessel, S., *Appl Catal. A: General* **96,** 253 (1993).
4. Zowtiak, J. M., and Bartholomew, C. H., *J. Catal.* **83,** 107 (1983).
5. Reuel, R. C., and Bartholomew, C. H., *J. Catal.* **85,** 63 (1984).
6. Castner, D. G., and Santilli, D. S., *in* "Catalytic Materials; Relationship between Structure and Reactivity" T. E. Whyte, R. A. Dalla Betta, E. A. Derovane, and R. T. K. Baker, Eds., ACS Symposium Series 248, p. 39. Am. Chem. Soc., Washington, DC, 1984.
7. Reuel, R. C., and Bartholomew, C. H., *J. Catal.* **85,** 78 (1984).
8. Iglesia, E., Soled, S. L., and Fiato, R. A., *J. Catal.* **137,** 212 (1992).
9. Rosynek, M. P., and Polansky, C. A., *Appl. Catal.* **73,** 97 (1991).
10. Bartholomew, C. H., and Farrauto, R. J., *J. Catal.* **45,** 41 (1976).
11. Roe, G. M., Ridd, M. J., Cavell, K. J., and Larkins, F. P., *in* "Methane Conversion," D. M. Biddy, C. D. Chang, R. F. Howe, and S. Yurchak Eds., Studies in Surface Science and Catalysis, Vol. 36, p. 509, Elsevier, New York, 1988.
12. Sexton, B. A., Hughes, A. E., and Turney, T. W., *J. Catal.* **97,** 390 (1986).
13. Mehanjiev, D., and Dimitrova, P., *Commun. Dep. Chem. Bulg. Acad. Sci.* **14,** 330 (1981).
14. Mehanjiev, D., Dimitrova, P., and Dyakova, B., *Commun. Dept. Chem. Bulg. Acad. Sci.* **17,** 204 (1984).
15. Chim, R. L., and Hercules, D. M., *J. Phys. Chem.* **86,** 3079 (1982).
16. Chin, R. L., and Hercules, D. M., *J. Phys. Chem.* **86,** 360 (1982).
17. Arnoldy, P., and Mouljin, J. A., *J. Catal.* **93,** 38 (1985).
18. Paryjczak, T., Ryunkowski, J., and Karski, S., *J. Chromatogr.* **188,** 254 (1980).
19. van't Blik, H. F. J., Konningsberg, D. C., and Prins, R., *J. Catal.* **97,** 210 (1986).
20. Hock, A., Post, M. F. M., Minderhoud, J. K., and Lednor, P. W., U. S. Patent 4,499,209, 1985, assigned to Shell.
21. Sault, A. G., *Appl. Surf. Sci.* **74,** 249 (1994).
22. Wagner, C. D., *in* "Practical Surface Analysis by Anger and X-ray Photoelectron Spectroscopy," D. Briggs and M. P. Seah, Eds., p. 477, Wiley, New York, 1983.
23. Chuang, T. J., Brundle, C. R., and Rice, D. W., *Surf. Sci.* **59,** 413 (1976).
24. Brundle, C. R., Chuang, T. J., and Rice, D. W., *Surf. Sci.* **60,** 286 (1976).
25. Haber, J., and Ungier, L., *J. Electron. Spectrosc. Relat. Phenom.* **12,** 305 (1977).
26. Mansour, S. A. A., *Mater. Chem. Phys.* **36,** 317 (1994).
27. Greenwood, N. N., and Earnshaw, A., "Chemistry of the Elements," p. 387, Pergamon Press, New York, 1984.
28. Mott, N. F., "Metal–Insulator Transitions," p. 138, Taylor & Francis, New York, 1990.
29. Dimitrova, P. G., and Mehanjiev, D. R., *J. Catal.* **145,** 356 (1994).
30. Kohler, S., Jackson, N., and Harrington, M., in preparation.
31. Coulter, K. E., and Sault, A. G., in preparation.